Combined Tangential-Normal Injection into a Supersonic Flow

P. S. King,* R. H. Thomas,† and J. A. Schetz‡
Virginia Polytechnic Institute and State University, Blacksburg, Virginia 24061
and
F. S. Billig§
Applied Physics Laboratory, Johns Hopkins University, Laurel, Maryland 20707

A combination of tangential and normal air injection into a Mach 3 airflow was experimentally studied. A rearward facing slot producing tangential injection at a nominal Mach number 1.7 was operated at several different total pressures. An array of transverse tubes of height equal to the slot height and placed just downstream of the slot was operated at two dynamic pressure ratios at both Mach 1 and 2.2. Mean flow measurements of static and total pressures were taken up to 20 slot heights downstream from which Mach number, density and velocity profiles, and entrainment rates were calculated. Various dimensions and spreading angles of the mixing regions were measured directly from nanoshadowgraphs and spark schlieren photographs. Large eddy structures were produced in several cases, leading to increased entrainment of the freestream. For some cases, heated air was injected through the normal tubes, and the jet total temperature decay was measured downstream. It can be seen from the data that the mixing rate can be significantly increased by the combined tangential-normal injection design over tangential slot injection alone, with up to 92% more entrained mass.

Nomenclature

d_N = normal injection tube outside diameter
d_N^* = normal injection tube throat diameter
H = slot injector height (nominally 0.5 in.)
L = left side (behind injection tubes)
$\dot{m}$ = mass flow rate
M = Mach number
p = pressure
$p_{N_{eb}}$ = normal jet effective back pressure, $0.8p_2$
$\bar{q}$ = dynamic pressure ratio, $(\rho u^2)_N/(\rho u^2)_\infty$
R = right side (between injection tubes)
s = normal injection tube spacing
T = temperature
u = velocity
W = width of test section (9 in.)
x = distance downstream from slot
$\tilde{x}$ = distance downstream from tubes
y = height above floor
δ = boundary-layer thickness
Δ = thickness of total mixing layer
Θ = nondimensional temperature
ρ = density
ρu = mass flux

Subscripts

0 = stagnation quantities
1,4 = station numbers
2 = conditions behind normal shock in flow
∞ = freestream
c = cone static probe
e = entrained
ex = exit pressure
i = initial condition (station 1R)
N = normal injection
T = tangential injection

Presented as Paper 89-0622 at the AIAA 27th Aerospace Sciences Meeting, Reno, NV, Jan. 9-12, 1989; received March 31, 1989; revision received Nov. 21, 1989.

*Graduate Research Assistant, Department of Aerospace and Ocean Engineering. Student Member AIAA.
†Research Associate, Department of Aerospace and Ocean Engineering. Member AIAA.
‡W. Martin Johnson Professor and Department Head, Department of Aerospace and Ocean Engineering. Fellow AIAA.
§Chief Scientist and Associate Supervisor, Aeronautics Department. Fellow AIAA.

Introduction

THROUGHOUT the continuing development of the scramjet concept, the mixing of fuel and air in the combustor has been one of many important and persistent problems. In the high Mach number range of flight, combustor velocities are of the order of 10^4 ft/s. The length of the combustor must be limited to a few feet due to the impact that the size of the combustor can have on the overall performance of a highly integrated hypersonic flight vehicle. Therefore, sufficient entrainment and subsequent micromixing followed by significant heat release must all occur in roughly 10^{-4} s.[1] Also, both the initial entrainment and micromixing are significant problems at high Mach number due to the inherently low rate of free shear layer mixing at these conditions. Clearly, these constraints dictate increased efforts aimed at improving the understanding of high Mach number mixing and mixing augmentation.

The difficulties of achieving adequate mixing at high Mach numbers are far from being well understood. Responsible mechanisms include the effect of eddy shocklets and the effect of compressibility on turbulent mixing.[1-4] Efforts to augment high speed mixing usually revolve around three-dimensional effects aimed at increasing the total area available for mixing, the introduction of longitudinal vorticity,[5] and shock interactions or oscillating shocks.[2] The understanding of efficient mixing processes also has many other applications, including thermal protection of surfaces and reduction of skin friction.

Many mixing augmentation schemes that are employed in subsonic flow fail to work at high Mach numbers, including the addition of swirl and acoustic noise. There are, however, several injection schemes for supersonic flow that do show promise, including injection from a strut and injection from wall surfaces. Struts can cause blockage and large total pressure losses in the flow and are not considered in this experiment. Two common types of fluid injection from the wall of a supersonic combustor include normal injection[6,7] from circular jets, for example, and tangential injection from a rearward facing slot.[8-10] In general, the advantages of tangential injection include a film cooling effect on the wall of the combustor and relatively low freestream total pressure loss,

since there is little flow disturbance. Also, since the injection is in the flow direction, significant thrust can be produced from the momentum of the injected fluid. However, without three-dimensional effects, the mixing rate is considered too slow. In comparison, normal injection is considered to have a much faster mixing rate and the benefit of penetration into the freestream. The larger freestream disturbance that normal injection creates can result in significant total pressure losses. Recirculation zones upstream and downstream of the injector create hot spots on the combustor wall. Also, with a normal injection scheme no thrust is derived from the momentum of the injected fuel. Injection at a downstream angle between 0 and 90 deg has various combinations of these advantages and disadvantages.[11]

In this research, experimental results are presented for a design that combines both tangential and normal injection schemes in a manner that seeks to include the advantages and to minimize the disadvantages of each. The normal injection was from an array of tubes equal in height to and located just downstream of a tangential slot in order to get maximum penetration while being sheltered from the hot freestream and to remove the hot recirculation zones from the surface of the slot lip. In addition, it is reasonable to expect that the combination of the bow shock from the normal jets, the jets, and the disturbance of the tubes themselves can create a favorable interaction with the freestream and slot flow to augment the mixing process above that of a slot alone.

Although a complete study of a fuel injection model should include injection of a low molecular weight foreign substance into the main flow, much can be learned from a "basic" study using only the injection of air. This simplifies the data reduction and the necessary equipment considerably. That plan was followed here.

Parameters varied in this experimental program included the slot and normal jet total pressures and the normal jet Mach number. The air injected normally was also heated for several cases in order to trace the path of the jet flow and to measure its temperature decay in order to assess its mixing rate. Mean flow measurements of cone-static pressure, total temperature, and pitot pressure were taken at a series of downstream stations. From these data, profiles of Mach number, density, and velocity were obtained. From the density and

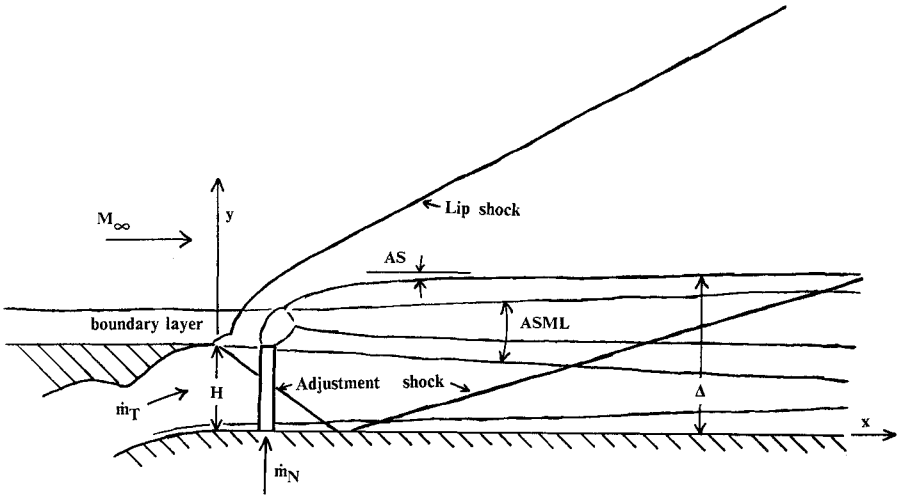

Fig. 1a Combined injection model, side view (not to scale).

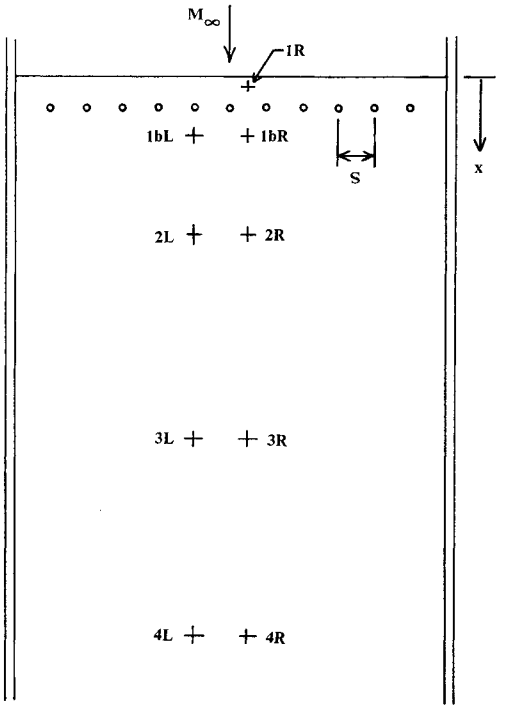

Fig. 1b Combined injection model, top view (not to scale).

velocity, mass flux profiles and entrainment rates were calculated. Schlieren pictures and nanoshadowgraphs were also taken to visualize the flowfields.

Experimental Apparatus and Methods

Model

All tests were performed in the Virginia Tech Supersonic Wind Tunnel. This blowdown facility provided run times of about 13 s at a freestream Mach number of 3, at a total pressure of 95 psia, and at a total temperature of 520°R, giving a freestream Reynolds number of 1.57×10^7 per foot. This test section was 4.5 in. high by 9 in. wide and over 1 ft long in the streamwise direction. The dimensions of the test section are on the same order as the size of an actual scramjet combustor.

The combined tangential-normal injection model is sketched in Fig. 1. The tangential injection consisted of a 0.475-in. high opening, rearward-facing slot injector separated from the freestream by a splitter plate 0.021 in. thick. (A nominal slot height of $H = 0.5$ in. was used to nondimensionalize many of the lengths in the experiment.) The contoured, converging-diverging slot injector was designed to operate nominally at a Mach number of 1.7 and total pressure of 10.7 psia.

The normal injection came from a row of 11 evenly spaced ($s/d_N^* = 17.4$) circular tubes located at $x/H = 0.5$ downstream of the slot. This large lateral spacing of jets was chosen to give a three-dimensionality to the flow to increase the available mixing area over that of a two-dimensional planar jet and to ensure that the three-dimensionality would persist far downstream until the jets merge by the last station. These tubes are equal in height to the slot and inject air normal to the freestream flow. Both sonic ($M_N = 1$) and supersonic ($M_N = 2.2$) jets were tested, each with a throat diameter $d_N^* = 0.043$ in. The sonic tubes had an outside diameter of $d_N = 0.0625$ in., while the supersonic tubes were twice as large at $d_N = 0.125$ in. A heating unit was developed to allow normal jet total temperatures of up to 660°R to be achieved, allowing the penetration and decay of the jet to be measured.

Test Matrix

The combined injector model was operated at several different operating points in order to study the effects that various parameters had on the flow. Many of the cases that showed typical trends and features are tabulated in Table 1 and are discussed in this paper. Both the tangential and normal injection systems allowed for variable total pressures (and hence mass flows). Case B, $M_N = 1$, $p_{0_N} = 350$ psia, and $p_{0_T} = 10.7$ psia, is considered to be the "baseline" case, and most other combinations of parameters are compared to this.

The tangential slot injector was run at a total temperature of 520°R and total pressures from 9.7 psia to 13.7 psia in 0.5 psi increments, resulting in exit pressures from slightly below to slightly above the freestream static pressure of about 2.6 psia. Thus, the slot injection ranged from slightly overexpanded to underexpanded, turning the external stream either toward or away from the wall after the step. The mean flow ρu profiles at the first station were integrated to give a baseline slot mass flow rate of 0.019 slugs/s. Measurements were also taken for cases with the tangential slot closed, so that the mixing of the transverse jets alone could be measured.

The normal injection was run at nominal total pressures of 350 and 500 psia, referred to hereafter as the "low pressure" and "high pressure" cases. The baseline mass flow from these injectors was measured to be 0.0031 slugs/s, giving a mass flow ratio $\dot{m}_N/\dot{m}_T = 0.16$. The high-pressure case had a higher mass flow at $\dot{m}_N = 0.0049$ slugs/s, or $\dot{m}_N/\dot{m}_T = 0.26$. Again, cases were run with no normal injection, so that the influence of the tubes themselves could be studied.

Measurements of pitot pressure, cone-static pressure, and total temperature were made at a series of nine stations in the flow. Five axial stations at $x/H = 0.25$, 1, 4, 10, and 20, referred to hereafter as stations 1, 1b, 2, 3, and 4, allowed the flow quantities to be measured as the mixing progressed downstream, see Fig. 1b. Two transverse measuring locations were used, one directly downstream of a normal jet (the left side) and the other midway between two jets (the right side). Therefore, the stations are referred to, for example, as station 1bL or station 3R. No data could be taken at station 1L. No profiles were taken of the flow upstream of station 1.

Data Reduction

The raw data were in the form of pitot pressure p_{0_2}, cone-static pressure p_c, and total temperature T_{0_2}. The data were reduced to profiles of Mach number, velocity, and density in the following manner.

For regions where the freestream Mach number was less than 1.2 (i.e., $p_c/p_{0_2} > 0.4782$), the shock wave on the cone-static probe became detached, and a locally constant value of static pressure p across the shear layer in these regions was assumed. Once the Mach number profile is found, T_{0_2} can be used to calculate density and velocity. These mean density and velocity profiles will then be integrated to yield mass flux at a given station. Using the value of the total mixing layer height, Δ, measured from the schlieren photographs, the mass flux in the total mixing layer at any station was found from

$$\dot{m} = H \int_0^{\Delta/H} \rho u \, \mathrm{d}\left(\frac{y}{H}\right)$$

By multiplying by the width of the test section (0.75 ft), the mass entrained into the total mixing layer can be calculated. Although this is a two-dimensional "strip" calculation done on both the left and right sides (behind and between the tubes), the average of the two sides should give a reasonable

Table 1 Injection conditions

	M_N	p_{0_N}	p_{0_T}	$\frac{u_T}{u_\infty}$	$\frac{(\rho u)_T}{(\rho u)_\infty}$	$\bar{q}$		$\frac{p_{N_{ex}}}{p_{N_{eb}}}$	$\frac{u_N}{u_\infty}$		$\frac{(\rho u)_N}{(\rho u)_\infty}$	
Jet temp.	Both	Both	Both	Both	Both	Cold	Hot	Both	Cold	Hot	Cold	Hot
Case A	1.0[a]	___	10.7	0.75	0.36	___	___	___	___	___	___	___
B	1.0	350	10.7	0.75	0.36	7.0	7.9	8.6	0.51	0.54	13.7	14.6
C	1.0	500	10.7	0.75	0.36	11.4	12.8	12.3	0.51	0.54	22.3	23.7
D	2.2[a]	___	10.7	0.75	0.36	___	___	___	___	___	___	___
E	2.2	350	10.7	0.75	0.36	6.1	6.8	1.5	0.87	0.93	6.9	7.3
F	2.2	500	10.7	0.75	0.36	9.8	11.0	2.2	0.87	0.93	11.1	11.8
G	1.0	350	9.7	0.75	0.32	7.0	7.9	8.6	0.51	0.54	13.7	14.6
H	2.2	350	9.7	0.75	0.32	6.1	6.8	1.5	0.87	0.93	6.9	7.3
I	1.0	350	12.7	0.75	0.42	7.0	7.9	8.6	0.51	0.54	13.7	14.6
J	2.2	350	12.7	0.75	0.42	6.1	6.8	1.5	0.87	0.93	6.9	7.3

[a] Presence of jet tubes but no normal mass flow.

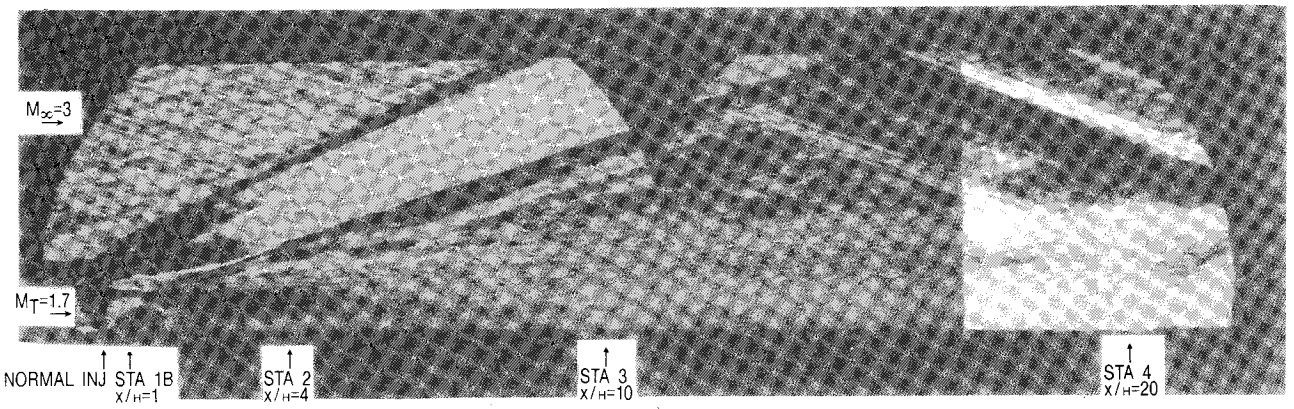

Fig. 2 Schlieren photograph of case B.

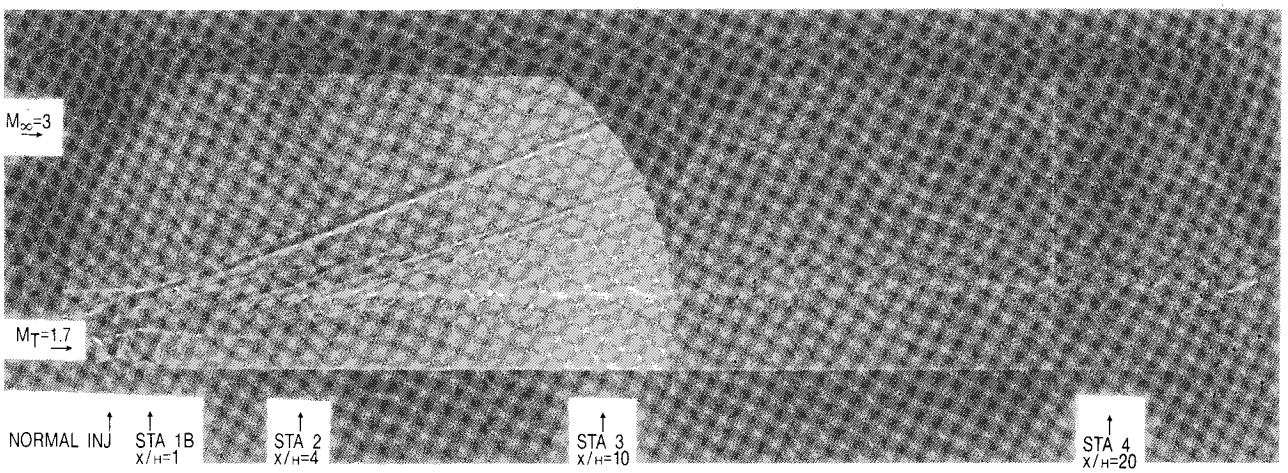

Fig. 3 Nanoshadowgraph of case A.

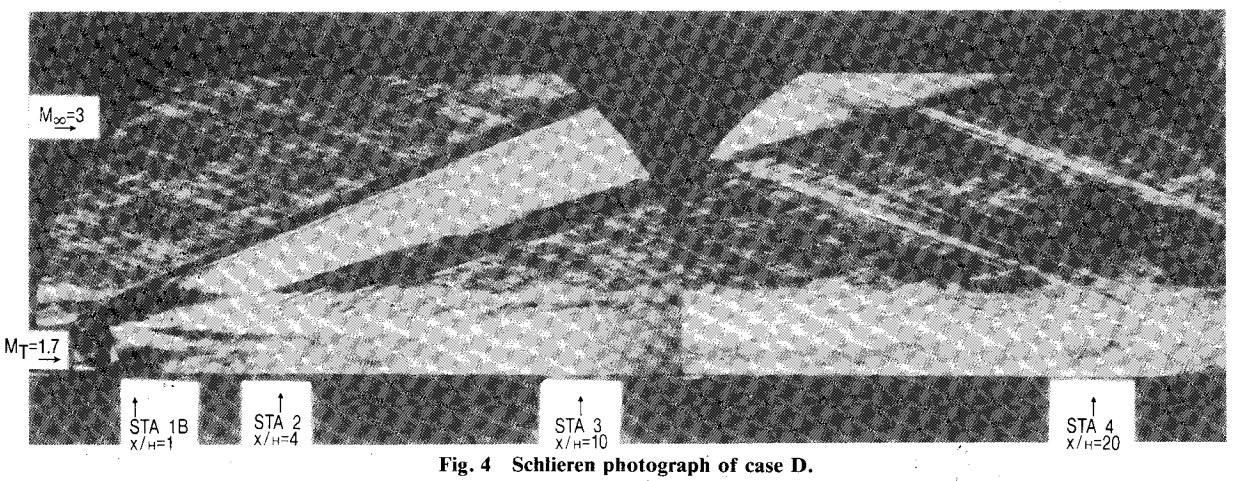

Fig. 4 Schlieren photograph of case D.

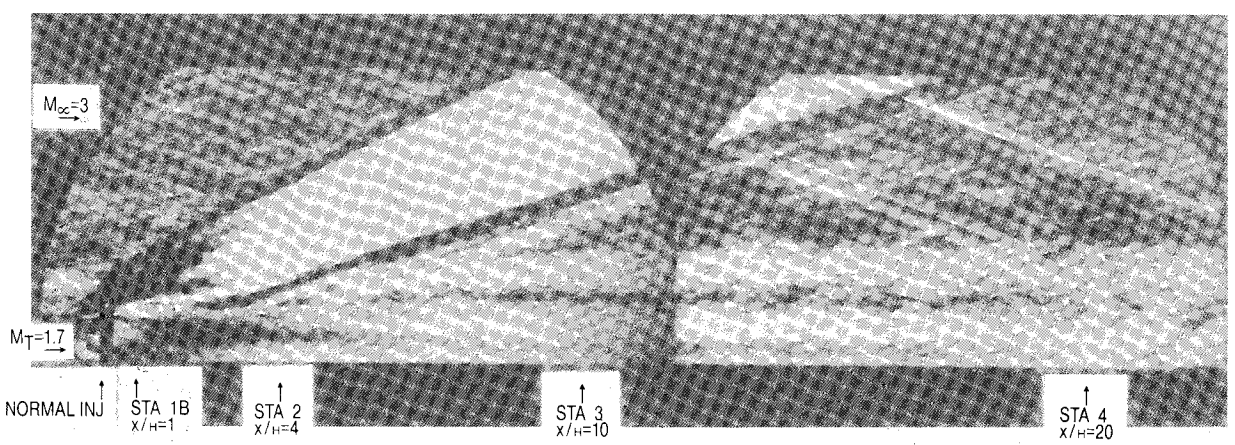

Fig. 5 Schlieren photograph of case F.

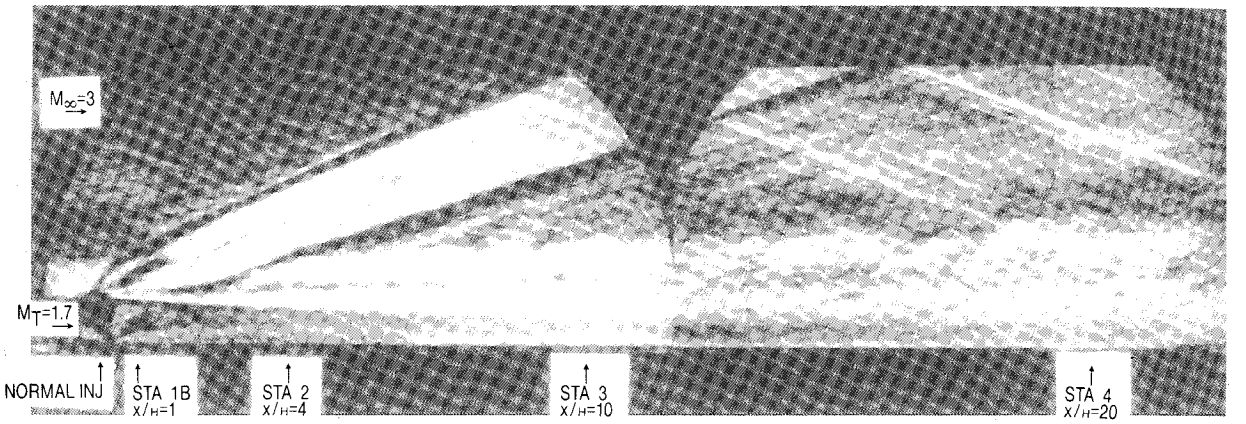

Fig. 6 Schlieren photograph of case G.

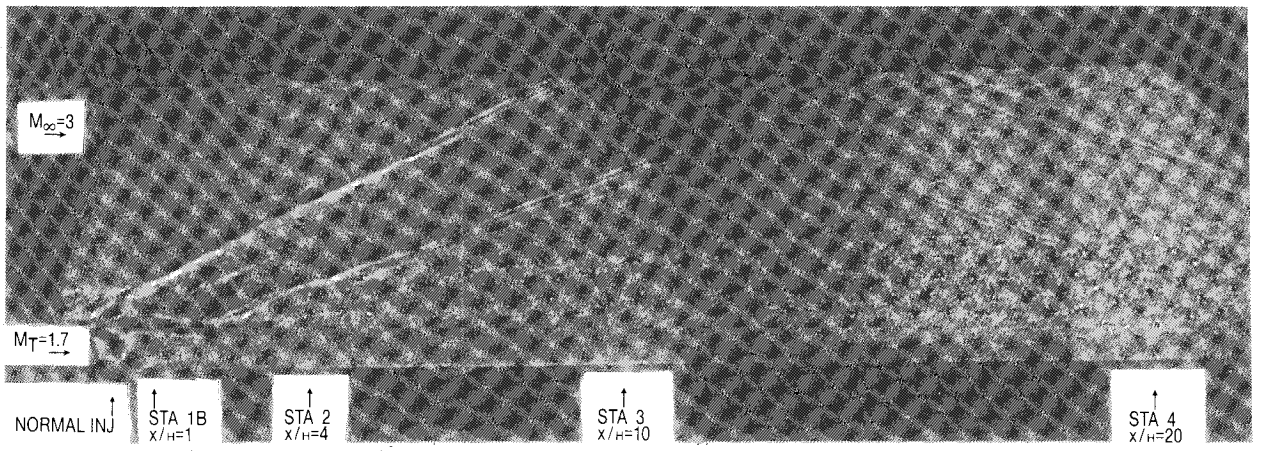

Fig. 7 Nanoshadowgraph of case G.

estimate of the mass entrained into the three-dimensional flowfield.

Results and Discussion

Photographs

Schlieren photographs and nanoshadowgraphs were made of the injection scheme under the different operating conditions tabulated in Table 1. Many of the important flow features can be seen in the photographs of Figs. 2–7. Although these photographic techniques are essentially two-dimensional, many interesting three-dimensional flow features, such as eddies and shocks, can be seen clearly. Since the schlieren photos have longer exposure times (10^{-6} s) than the nanoshadowgraph (10^{-8} s), they show the mean flow features more clearly. The nanoshadowgraphs do a much better job of "freezing" the flow, making it easier to see the fine structure and turbulence. Also, shadowgraphs of any time exposure show shocks more clearly. However, dimensions taken from individual nanoshadowgraphs can be misleading, since they capture transient flow features at only one instant of time. Therefore, Table 3 includes only measurements taken from the schlieren photographs.

Figure 2 is a schlieren photograph of the flow at baseline conditions, case B. The flow is from left to right. The rearward facing slot can be seen at the lower left in this and later photos. The boundary-layer thickness on the freestream side of the splitter plate δ_i is about 0.3 in. An adjustment shock and lip shock can be seen emanating from the splitter plate. The adjustment shock hits the floor near the injection tubes and reflects up into the freestream. Also seen is the array of normal injection tubes downstream of the slot. The bow shock from the normal jets is also clearly visible. The flow in the region near the injection tubes is very complex and three-dimensional and therefore shows up dark in the schlieren photo due to the large density gradients. Also, the schlieren system acts to integrate these gradients across the test section, further blurring this region. However, three distinct turbulent layers can be seen growing and eventually merging downstream of the slot. The first of these is the lower wall boundary layer downstream of the slot. This layer is responsible for the wall cooling effect of the slot flow, which in a real combustor would be much cooler than the incoming supersonic air. Next, going upward is the splitter plate mixing layer coming off the slot lip where the freestream and the slot flow begin mixing. This layer includes the incoming upstream wall boundary layer and the splitter plate wake. Above these two layers is the jet layer produced by the injection through the normal tubes. Although the array of jets is very three-dimensional, Fig. 2 clearly shows the penetration and spreading of the jets as they are turned and travel downstream.

The rate at which these layers grow and merge is a prime indicator of the overall effectiveness of this injection scheme. Improved mixing schemes would be indicated by increases in the spreading angles and thicknesses of the various layers. These dimensions, shown in Fig. 1a, were measured from the schlieren photographs and are tabulated in Table 2. The distance from the floor to the top visible edge of the jet layer is referred to as the total mixing layer height, Δ. The angle of spread of this total mixing layer measured between stations 3 and 4 is $AS_{3\text{-}4}$, while $ASML_{2\text{-}4}$ is the angle of spread of the splitter plate mixing layer, measured between stations 2 and 4. The length before the splitter plate mixing layer and the floor boundary layer merge, nondimensionalized by H, is denoted LBM. The apparent length LBM depended somewhat on the exposure setting of the camera system, and the actual point of merging was sometimes hard to measure precisely from the photos.

Figure 3 is a typical nanoshadowgraph of the flow for case A. It can be seen that the bow shock produced by the normal injection tubes is at a lower angle, since there is no normal

mass flow. Also, the total mixing layer thickness, Δ, is everywhere less than for the cases with normal injection, and it remains nearly constant as evidenced by the low value of $AS_{3\text{-}4}$. Note that the flowfield does not appear as complicated in this nanoshadowgraph as it did in the previous schlieren photograph. Also, the downward deflection of the freestream into the overexpanded slot flow can be seen.

Figure 4 is a schlieren photo that shows the flow for case D with no normal injection, but with the array of supersonic injection tubes in place of the sonic injectors. The larger outside diameter of these tubes is clearly visible. Cases with no normal injection have only two mixing layers. Figure 5 is a schlieren photograph of high pressure, supersonic normal injection, case F. The jet layer is visible penetrating higher above the splitter plate mixing layer than for the sonic jets. Also visible is the spread and breakup of the jet as it becomes more turbulent. By station 4, the jet and the splitter plate mixing layer have started to mix together. Again, it is seen in Table 2 that normal injection increases Δ and $AS_{3\text{-}4}$. Increases in Δ are to be expected due to penetration of the normal jet into the freestream, but the increases in $ASML$, and possibly AS as well, could be due to the augmentation of mixing that the combined injection design has over tangential slot injection alone.

Figures 6 and 7 show a schlieren photograph and nanoshadowgraph of case G. This case is similar to case A but with a slightly lower value of the slot total pressure. These photographs are included to show a more interesting flow feature. Relatively large, periodic eddy structures are generated in the jet plume and, to a lesser degree, in the splitter plate mixing layer. These eddies were found to vary in strength with differing values of the slot total pressure. They were barely noticeable at $p_{0_T} = 10.7$ psia and appeared most strongly around $p_{0_T} = 9.7$ psia and $p_{0_T} = 12.7$ psia. The strength of the eddies decreased on either side of these values. Measurements from Fig. 6 indicate an eddy structure angle of about 40 deg in the region from $x/H = 7$ downstream until the jet and splitter plate mixing layer are better mixed. In Fig. 7, the fine scale turbulence of the mixing region is more evident. The angle of the axis of the large eddy structures in this photograph was found to be 60 deg relative to the freestream near station 3 and decreased with downstream distance. The diameter of these structures was on the same order as H and δ_i. The schlieren and nanoshadowgraph photographs for this case indicate an average structure diameter of around $0.6H$ and average wavelength of $0.4H$. Structures found in case I had an average diameter of $0.5H$ and an average wavelength of $0.6H$. These structures were also seen in some supersonic normal injection cases. In Table 2, it can be seen that case G has the largest spreading angle $AS_{3\text{-}4}$ and among the largest value of Δ_4/Δ_i. The value of LBM for this case does not decrease as might be expected, but was lower for some other cases where these structures were seen. By comparison, the spreading angles of the slot alone are very small as would be expected, since the exit pressure of the slot is almost matched to the freestream pressure.[11,12] The disturbance that the tubes create, even without any normal mass flow, has a significant effect on the growth of the splitter plate mixing layer. This could be because the supersonic normal injection tubes have a larger outside diameter than the sonic injectors, causing the shedding of vortices of a different size and frequency. Case H has mixing layer dimensions similar to case G, except for the value of $AS_{3\text{-}4}$, which is only half of the case G value. The eddy structures were not seen in this case. Case I photos also showed these large eddy structures, although it has spreading angles and mixing layer thicknesses more typical of the no injection cases A and D. Case J did not have these structures and has spreading parameters similar to case I.

Table 2 Parameters measured from schlieren photographs

Case	Δ_i/H	Δ_4/Δ_i	$ASML_{2\text{-}4}$, deg	$AS_{3\text{-}4}$, deg	LBM
A	1.6	1.1	1.1	1.5	16
B	1.3	1.8	2.3	1.8	13
C	1.5	1.7	2.0	2.1	14
D	1.7	1.2	1.1	1.0	22
E	1.7	1.4	0.9	0.8	20
F	1.7	1.5	1.1	1.5	19
G	1.6	1.5	1.3	2.0	18
H	1.5	1.6	1.2	1.0	19
I	1.6	1.5	1.1	1.7	20
J	1.6	1.5	1.2	1.4	18
Slot alone	1.7	1.1	0.5	1.4	23

The cases with the larger thicknesses and spreading angles shown in Table 2 indicate some important trends. First of all, it can be seen that the value of Δ_4/Δ_i and $AS_{3\text{-}4}$ are related, since an increase in $AS_{3\text{-}4}$ generally leads to a larger value of Δ_4 (see Fig. 1a). Likewise, an increase in $ASML_{2\text{-}4}$ leads to a decrease in LBM. The value of $ASML$ and LBM are influenced by the interaction of the jet and splitter plate mixing layers. For the sonic, $p_{0_T} = 10.7$ cases, A-C, the value of $ASML_{2\text{-}4}$ increases with the addition of normal injection. The low-pressure case had an increase of 109% over the no normal injection case, while the high-pressure case was just 82% larger. This may be due to the fact that the high-pressure jet penetrates the incoming boundary layer farther and hence mixes with its slightly less than the low-pressure jets. By station 1, the baseline sonic jet had a penetration of only $1.4H$, while the baseline supersonic jet penetrated over 1.6 slot heights. The incoming boundary layer was on the order of $0.6H$ so that its outer edge is at $1.6H$. Farther downstream, the sonic jet still had not penetrated much beyond this, while the supersonic jet had reached a height of almost $2H$. For the supersonic jet cases, D-F, as well as the sonic cases G and H, there is little change in the value of $ASML_{2\text{-}4}$. The values of $ASML_{2\text{-}4}$ for cases I and J are about the same as for the no normal injection cases. The values of LBM for these cases follow similar trends.

The trends of $AS_{3\text{-}4}$ and Δ_4/Δ_i may give a better indication of mixing, since they represent the growth of the entire mixing layer. These values are strongly influenced by the penetration of the jet and its interaction with the incoming boundary layer. Again, the values in Table 2 indicate an increase in the spreading angle $AS_{3\text{-}4}$ and thickness Δ_4/Δ_i with the addition of normal injection. Low and high pressure sonic injection increased $AS_{3\text{-}4}$ by 20% and 40%, respectively, over the no normal injection case, while Δ_4/Δ_i increased by 64% and 55%. For cases D-F, the supersonic normal injection decreased $AS_{3\text{-}4}$ by 20% for the low-pressure case and increased it by 50% in the high-pressure case compared to the no normal injection case. The Δ_4/Δ_i was increased only 17% and 25%, respectively, for these cases. However, for case G in the presence of the large eddy structures, $AS_{3\text{-}4}$ increased 54%, whereas Δ_4/Δ_i increased 18% over the corresponding no normal injection case. For case I, the value of $AS_{3\text{-}4}$ is around the same as for the other sonic low-pressure cases. The Δ_4/Δ_i for this case is also not increased above the other cases. Case J had very similar dimensions. Notice that the slot alone flow dimensions show less mixing than practically every other case, even the ones without normal injection. From these photographic results, it can be concluded that the sonic, low-pressure injection produced the best combination of spreading angles and mixing layer growth. The presence of the large eddy structures seemed to produce an increase only in $AS_{3\text{-}4}$, not in the total mixing layer thickness.

Mean Flow Profiles

The raw pressure and temperature data were reduced as discussed earlier and plotted vs the height above the lower wall. The velocity and density profiles were nondimensionalized by their local freestream values. This section will concentrate mainly on descriptions of the Mach number profiles,

since the velocity and density profiles usually show similar features. Due to space limitations, profiles are only presented for a few cases. Readers interested in a more complete set of profiles should see Ref. 13.

Figure 8 is a plot of Mach number vs the height above the wall at stations 1bL through 4L for case A. Recall that the left side stations are located behind the tubes and the right side stations are downstream between the tubes. The incoming freestream and slot flows are visible at station 1b, although somewhat disturbed, because this station is close behind the normal injection tubes. As the flow proceeds to stations 3 and 4, the profiles smooth somewhat and approach a fully developed turbulent boundary-layer shape. Figure 8 also shows a much cleaner freestream and slot flow at station 1 on the right side between the tubes. From this profile, it is seen that the slot Mach number is less than the nominal value of 1.7. The initial freestream boundary layer is about $0.6H$ thick. The lower wall boundary layer as well as the splitter plate mixing layer and wake are easily recognized. Also, the slot flow does not merge with the freestream as well as on the right side, the profile being less fully developed by station 4. The data from this station (1R) was used as an initial condition in later entrainment calculations. The value of Δ_i was typically around $1.6H$. At station 2 in Fig. 8, the presence of the bow and lip shocks are seen at $y/H \simeq 2.7$ and 2, respectively. These two features were seen on many station 2 profiles, and they match up well with dimensions taken from the schlieren photographs.

Figure 9 gives plots of Mach number for case B. In this figure, it can be seen that there is a region near $y/H \simeq 1.3$ where the Mach number is indicated to be zero at station 1b. This occurs only on the left side profiles in the cases with normal injection. In this region, the calculated total pressure was found to be less than the assumed locally constant value of static pressure, a situation that is clearly impossible. This leads to the conclusion that perhaps flow angularity at this point directly behind the normal jet makes the measurement and data reduction techniques discussed earlier invalid. We believe these problems are mainly with the cone-static probe. Of course, this problem shows up in the velocity and density profiles for these cases also. In Fig. 9, the jet and splitter plate mixing layers are visible at station 2 as a peak in the Mach number profile. The location of this peak agrees with the schlieren photograph of this case (see Fig. 2). By station 4, the flow is more fully developed than in case A. By comparing the right and left side profiles at stations 3 and 4, one effect of the normal jets can be seen. The slot region is fuller for the flow between the jets. On the left side behind the tubes, the jet has pushed the region between the freestream and slot flow upwards. This will be discussed again in the entrainment section below. The profiles for case C are very similar to the profiles presented for case B. The main difference seems only to be a slight increase in the penetration of the jet layer.

For the rest of cases, D–J, data were collected at stations 4L and 4R only. In case D, the left and right profiles at station 4 are similar. There is no normal injection in this case, although the larger diameter supersonic tubes are in place. The total mixing layer thickness is slightly higher on the right side between the tubes. In case E, the total mixing layer thickness is increased on the left side by the addition of low-pressure normal injection. Again, the right side profile looks more fully developed than the left side, but with a smaller total mixing layer thickness, Δ. Case F profiles are very similar to case E

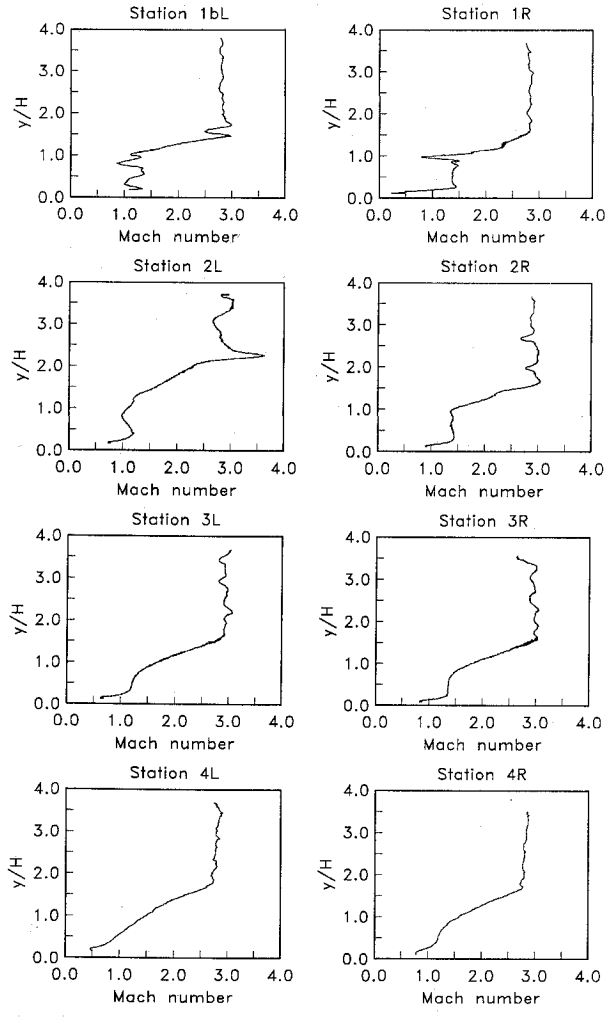

Fig. 8 Case A, sonic jets, $p_{0_T} = 10.7$ psi, no normal injection.

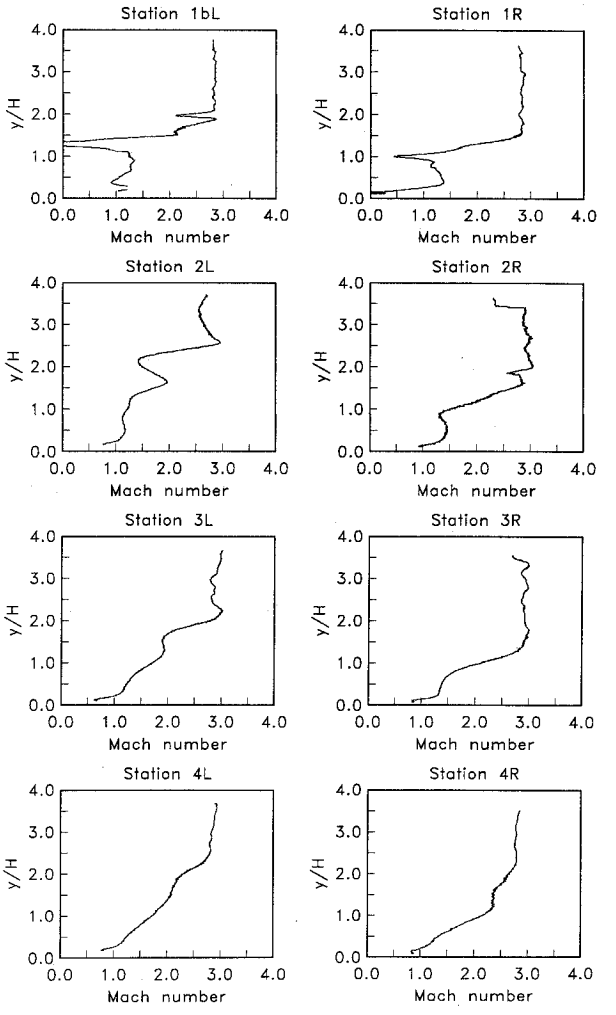

Fig. 9 Case B, sonic jets, $p_{0_T} = 10.7$ psi, $p_{0_N} = 350$ psi.

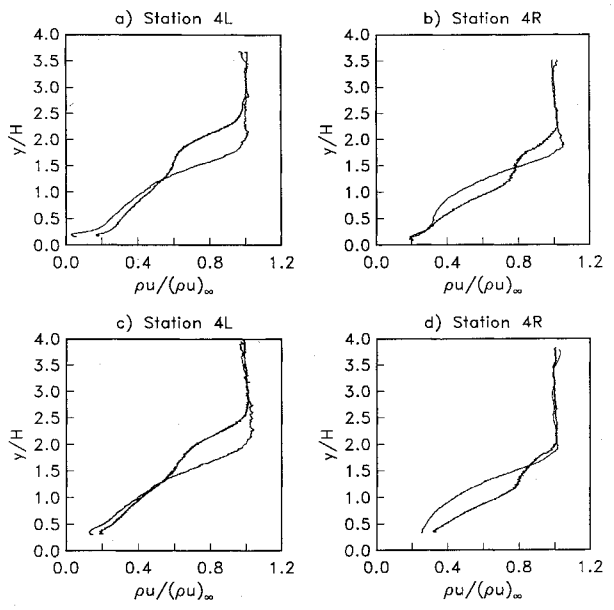

Fig. 10 Mass flux, sonic jets; a, b) cases A, B, $p_{0_T} = 10.7$ psi; c, d) case G, $p_{0_T} = 9.7$ psi.

profiles, except for the slightly increased penetration behind the tubes due to the higher jet total pressure.

Most of the mean flow profiles (except for ρu) computed for different slot and jet total pressures were similar in their basic shape at a given station and seemed to be relatively insensitive to these parameters as they were varied.

Entrainment

A measure of the mixing that occurs in this, or any, design is the amount of freestream air that is entrained into the total mixing layer. Typical mass flux profiles at station 4 for cases B and G have been plotted in Fig. 10. The different layers in the flow have penetrated and merged into the freestream somewhat by this station. Again, a more complete set of profiles is to be found in Ref. 13.

Mass flows were computed at the slot face (station 1R) and at station 4 by integrating the mean flow ρu profiles across the total mixing layer. From the cases without normal injection, A and D, there are only small differences between the left and right sides in the ρu profiles at station 4. There are significant differences, however, for both the low and high pressure injection cases (B, C, E–J). At first glance, it seems that the ρu profiles for the right side are more fully developed and, thus, have a larger integrated mass flux. But, the values of the total mixing layer thickness, Δ, for the left side are always larger than on the right side, giving a larger height of integration and making up for the apparent mass flux deficit seen in the profiles. Values of Δ for use in these calculations were taken as the height where the local velocity reached 99% of the local freestream velocity. These values taken from the left side agreed very closely to values measured from the schlieren photographs. However, total mixing layer thicknesses measured from the right side profiles were lower than in the photographs. This difference is because the flow is not two dimensional even at station 4 due to the large lateral jet spacing ($s/d_N^* = 17.4$), and the photographs indicate only the thickest part of the total mixing layer. It is expected, then, that Δ will be larger and that more mixing will occur directly behind the tubes, since the losses associated with the tube drag and wake usually enhance mixing. By taking the difference between the mass flow at station 4, $\dot{m}_4$, and the sum of the mass flows at $x/H = 0$ and the normal injected mass flow, $\dot{m}_i + \dot{m}_N$, the mass flow entrained into the total mixing layer across the width of the test section $\dot{m}_e$ could be obtained. The results of these calculations are shown in Table 3.

In this section, the performance of each case will be compared to the slot alone configuration. First, it is interesting to note that the entrained mass flow $\dot{m}_e$ for the slot alone is greater than for the case with tubes but no normal injection. This suggests that there are some losses associated with flow over the array of tubes. However, these losses occur mainly in the slot flow and do not contribute to mixing the freestream and slots flows together. Some estimates of these losses can be made. First, the thrust due to the slot flow was calculated in a similar fashion to the mass flow calculations discussed above. For the baseline case B, the slot thrust was calculated to be 22.9 lb. For the drag on the array of tubes, a drag coefficient of 1.45 for an infinite cylinder was used.[14] This gave a drag of only 0.17 lb per sonic tube, and 0.34 lb for the larger supersonic tubes. For the entire array of eleven tubes, then, a maximum drag of 3.7 lb was obtained. Thus, the tube array drag is seen to be only 16.3% of the slot thrust. Although this loss is not negligible, it is less than the gains achieved by increased mixing. This trend will be shown below. Another "loss" might be in the interaction of the turbulence produced by the tube array and that in the mixing layers. The scale of the tubes is a tenth of the scale of the incoming boundary layer and the largest eddy structures. Thus, the tubes themselves will not help in the production of eddies. More likely, the tubes contribute to the breakup of these large structures, enhancing the micromixing but decreasing the large-scale entrainment and mixing. Another measure of the losses associated with the normal injection arrangement is the total pressure drop across the tube/jet bow shocks. For the cases with no normal injection, the freestream total pressure at station 2 was calculated from the mean flow profiles to be 86.7 psia, for a total pressure drop of 9.2%. For the baseline, low-pressure injection cases, the station 2 total pressure was 90.9 psia, a drop of only 4.8%. Clearly then, the gains from this injection scheme can outweigh the losses.

It can be seen in Table 3 that for the cases with no normal injection, A and D, there is little difference between $\dot{m}_e$ for the left and right sides. The supersonic jet case D has a slightly higher value, possibly due to a greater disturbance caused by the larger injection tube diameter. However, when sonic normal injection is introduced, cases B and C, the entrained mass increases 194% compared to the slot alone for the low-pressure case, and 206% for the high-pressure case. The supersonic jets, cases E and F, increased $\dot{m}_e$ only 62% and 95% compared to the slot alone for the low- and high-pressure cases. What is perhaps more surprising is that the normal

Table 3 Results of mass entrainment calculations

Case	Side	$\dot{m}_4 W$	$\dot{m}_i \cdot W$	$\dot{m}_N$	$\dot{m}_e \cdot W$	$\frac{\Delta \dot{m}_e \cdot W}{\Delta x}$
A	L	0.050	0.035	___	0.016	0.019
A	R	0.049	0.035	___	0.014	0.017
B	L	0.088	0.038	0.003	0.047	0.057
B	R	0.080	0.038	___	0.043	0.052
C	L	0.089	0.036	0.005	0.049	0.056
C	R	0.091	0.036	___	0.056	0.068
D	L	0.056	0.035	___	0.021	0.026
D	R	0.046	0.035	___	0.011	0.013
E	L	0.074	0.038	0.003	0.034	0.041
E	R	0.082	0.038	___	0.044	0.053
F	L	0.082	0.036	0.005	0.041	0.050
F	R	0.085	0.036	___	0.049	0.060
G	L	0.101	0.036	0.003	0.063	0.077
G	R	0.083	0.036	___	0.047	0.057
H	L	0.077	0.036	0.005	0.038	0.046
H	R	0.079	0.036	___	0.044	0.053
I	L	0.085	0.041	0.003	0.041	0.050
I	R	0.084	0.041	___	0.043	0.052
J	L	0.084	0.041	0.005	0.038	0.046
J	R	0.091	0.041	___	0.050	0.061
Slot alone	___	0.074	0.041	___	0.033	0.040

injection also increased the entrainment on the right side, between the jets. In most cases, the right side showed a larger amount of mass entrained than the left side behind the jets. If the right and left side values are averaged, it is seen that the sonic injection increased $\dot{m}_e$ by 206% and 244% for cases B and C compared to the slot alone, while the Mach 2.2 supersonic jets increased it by 141% and 175% over the slot alone for cases E and F.

The entrained mass flow for case G, when the large eddy structures were present, shows a very large increase on the left side downstream of the tubes. The mass entrained in this case is about 2.3 times as large as the slot alone case[12] in the last row of Table 3. However, case I also had large eddy structures present in the jet layer, but did not show as large an increase in entrainment as case G. Case J, like case H, did not show evidence of the structures and had average values of entrained mass. Even the combined injection cases without evidence of large eddy structures show an increase in entrained mass over the slot alone.

These data show that entrainment of the freestream is greatly improved by use of the combined tangential-normal injection over the slot alone, especially at conditions where the turbulent eddy structures are present. The effectiveness of the tubes with normal injection compared to that without injection can be rationalized with the observation that the scale of the underexpanded jet plumes is much larger than that of the tubes and is of the same order of the large-scale structures in the mixing layers. Thus, the jet plumes can interact favorably with the large-scale structures.

Crocco and Lees[15] have estimated that the mass entrained into a two-dimensional boundary-layer-like flow is given by

$$\frac{d\dot{m}_e}{dx} \simeq c(\rho u)_\infty$$

where $0.01 < c < 0.03$. For $c = 0.02$, this equation gives a value of $d\dot{m}_e/dx = 0.047$ slugs/s/ft^2. Across the 9-in. (0.75 ft) width of the test section, there would be $(0.047)(0.75) = 0.035$ slugs/s/ft entrained into the mixing layer. Between stations 1 and 4 (0.82 ft), the entrained mass would be 0.029 slugs/s. This is slightly less than that found in the slot alone data in Table 3, shown that slot mixing is only slightly more effective than boundary-layer entrainment and mixing.

Except for varying the strength of the eddy structures and the subsequent mass that they help entrain, the slot total pressure seemed to have little effect on the rest of the flowfield. The effect of p_{0_T} is essentially that it adjusts the deflection of the freestream into the slot flow, changing the interaction of the slot flow with the tube/jet array. Again, some structure was observed for certain supersonic jet cases, resulting in a higher entrained mass flow. The supersonic jet cases without structures showed no significant increase over the sonic cases. All of this suggests that the scale of the added flow features with the tube/jet array and their location with respect to the other mixing layers are very important if one wishes to obtain mixing augmentation.

Jet Penetration and Decay

Total temperature profiles of heated normal injection taken downstream allowed the determination of the jet trajectory and temperature decay along the jet. The decay of the peak jet temperature gives a measure of external fluid entrained into the jet plume. When looking at the jet flow and its decay, the downstream stations are better described by their distance from the jet tubes, not from the slot. The left side stations 1bL through 4L are located at $\bar{x}/d_N^* = 6$, 41, 111, and 227, respectively. The temperature profiles have been nondimensionalized as

$$\Theta \equiv \frac{T_{0_2} - T_{0_\infty}}{T_{0_N} - T_{0_\infty}}$$

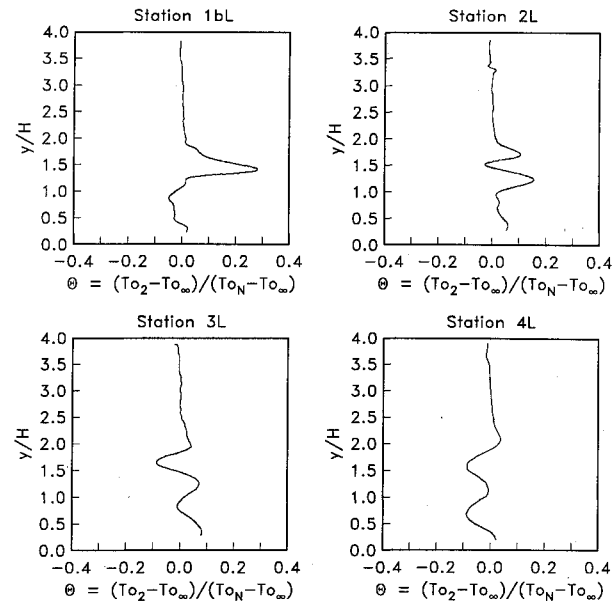

Fig. 11 Nondimensionalized temperature for heated normal injection, case B, sonic jets, $p_{0_T} = 10.7$ psi, $p_{0_N} = 350$ psi.

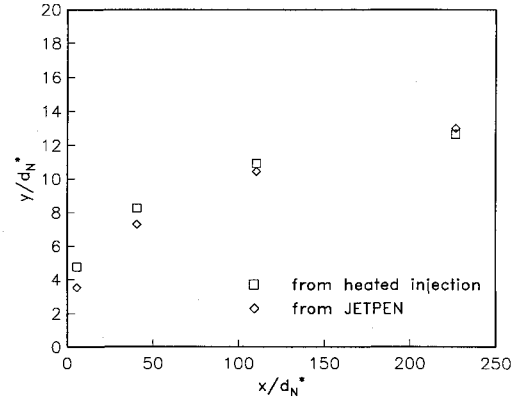

Fig. 12 Normal jet trajectories, case B.

which is a measure of the local total temperature increase due to the heated normal jet. Typical profiles of this quantity are shown in Fig. 11. They show the jet widening and its centerline temperature decreasing as the flow progresses downstream and cooler air is mixed into the jet. A second temperature peak can be seen below that of the jet plume, indicating that some of the heated jet mass flow is entrained in the splitter plate mixing layer immediately downstream of the tubes. At the downstream locations, the total temperature is indicated to be lower than that of the flow at the upstream locations. This is due to the mixing and spreading of the heated jet core and the fact that it is difficult to keep the total temperature of a blowdown facility constant. At several locations, the value of Θ is indicated to be below zero. This may be due to several factors. First, it is likely that the slot total temperature is lower than that of the freestream. Second, the wall temperature of the splitter plate is lower than the freestream temperature.

The jet trajectory and penetration into the freestream could be determined from the height of the peak jet temperature. Close agreement was found between these measurements and data computed from the JETPEN (JET PENetration) computer program,[16] especially as the jet progressed downstream. Figure 12 is a typical plot of these trajectories. They also agreed well with measurements taken from the schlieren photographs.

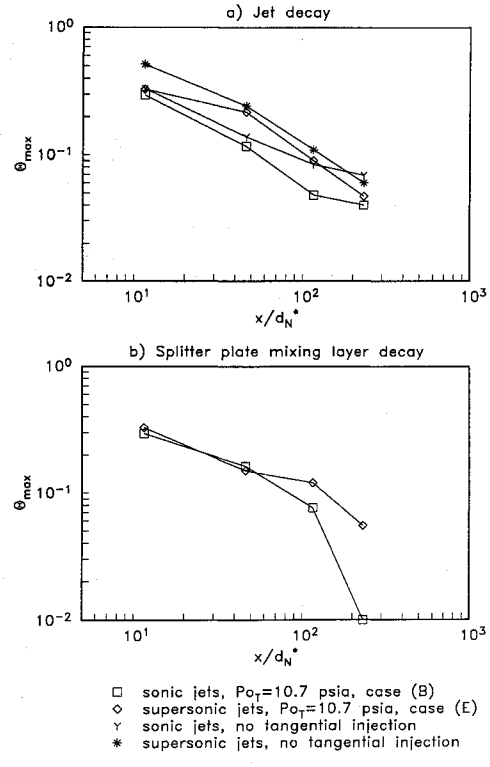

Fig. 13 The Θ_{max} decay, $p_{0_N} = 10.7$ psia.

Figure 13 is a plot of the maximum jet temperature decay for cases B and E, as well as for two cases with no tangential slot injection. It can be seen that there are two distinct regions of differing slopes, indicating two regions of decay. The upstream region extends from the injection tubes to about 40 d_N^* downstream and is characterized by a slower rate of mixing than in the downstream region. Better initial mixing is seen to be produced by the higher jet expansion ratio $p_{N_{ex}}/p_{N_{eb}}$ found in the sonic cases (see Table 1), where $p_{N_{eb}}$ is an "effective back pressure."[17] This is true for the jet alone cases as well as the combined tangential-normal cases. This parameter indicates how well the jet is matched to the exit conditions behind the bow shock. Since the supersonic jets have a value of $p_{N_{ex}}/p_{N_{eb}}$ closer to unity, they cause less disturbance to the flow, and hence, reduced interaction. The effect is less for the combined cases, because, for equal expansion ratios, the slot flow would also increase initial mixing. The effect of the jet to freestream dynamic pressure ratio $\bar{q}$ is similar; when $\bar{q}$ is higher (i.e., the supersonic cases), the jet penetrates beyond the incoming boundary layer and interacts with it less. The normal jet momentum flux ratio seems to have little effect on the jet decay. The higher mass flux ratios of the sonic cases may account for some of the increased initial mixing.

The apparent switch from an upstream mixing region to a downstream mixing region occurs at the point where the jet has lost most of its normal momentum. This increase in mixing rate could be due to the fact that the flow is then locally more like a coaxial mixing process. The rate of decay in the downstream region may be due to the difference in axial momentum in this region. The point at which the sonic cases seem to flatten out ($\tilde{x}/d_N^* \simeq 100$) is where the jet axial momentum is estimated to have approached that of the freestream.

Overall, the combined tangential-normal cases have faster initial mixing and somewhat faster downstream decay rates than do the slot or normal jets alone, resulting in significantly shorter lengths to reach desired mixing levels. Sonic jet cases seem to produce faster initial mixing than do supersonic jet cases. However, sonic injection mixing rates tend to flatten out after $\tilde{x}/d_N^* \simeq 225$, where the supersonic jet cases begin to produce faster mixing rates. There were no clear differences between the various slot total pressures tested.

The decay rates in the splitter plate mixing layer are also shown in Fig. 13. The trends are similar to those discussed above, although there seems to be less difference between the sonic and supersonic jets until the downstream region is reached. In the downstream region, however, the sonic jets produced far superior mixing in contrast to the situation in the jet plume flow above.

Conclusions

This experimental program was aimed at determining whether combined tangential-normal injection would have faster mixing rates than a tangential slot injector alone. The data presented here show that, indeed, the combined injection scheme is to be preferred over the slot alone.

From the photographic evidence, it was shown that the low- and high-pressure, sonic normal injection cases gave the largest improvement in total mixing layer thickness (an average of 60% improvement over the slot alone case) and in total mixing layer spreading angle $AS_{3\text{-}4}$ (an average of 30% improvement over the slot alone). Apparently, most of the gain in mixing is achieved by going from no normal injection to the low- or high-pressure case. The slight additional initial penetration of the jet into the freestream in the supersonic normal injection cases does not seem to increase the spreading angles or total mixing layer thickness substantially.

The entrainment calculations indicate that the high-pressure sonic injection cases gave the largest increase in the amount of freestream air entrained into the mixing layers. Up to 92% more mass was entrained compared to the slot alone case. The large eddy structures observed have been shown to be very desirable aids to mixing entrainment. When they were present in the jet flow, the entrained mass in that region increased substantially. Although both large-scale mixing and molecular mixing are required for combustion, the development of these large eddy structures is an important first step in developing augmented mixing schemes.

Results of the jet decay analysis again show that sonic normal injection is to be preferred over supersonic injection, with no real bias toward the low- or high-pressure cases.

Each of the different parts of this experimental analysis gives a different piece of the larger puzzle. Put together, it seems clear that this combined tangential-normal injection model shows considerable improvement over the slot injector alone and has great promise for further development and use.

A final important point clearly emerges from this study. This, or any, mixing augmentation scheme depends upon detailed interactions between various features of the flow. To achieve a helpful interaction, careful "tuning" is required.

References

[1]Ferri, A., "Supersonic Combustion Progress," *Astronautics and Aeronautics,* Aug. 1964, pp. 32-37.

[2]Kumar, A., Bushnell, D. M., and Hussami, M. Y., "A Mixing Augmentation Technique for Hypervelocity Scramjets," AIAA Paper 87-1882, 1987.

[3]Papamoschov, D., and Roshko, A., "Observations of Supersonic Free-Shear Layers," AIAA Paper 86-0162, 1986.

[4]Bogdanoff, D. W., "Compressibility Effects in Turbulent Shear Layers," *AIAA Journal,* Vol. 21, No. 6, pp. 926-927.

[5]Hersch, M., and Povinelli, L. A., "Injection into a Supersonic Stream from the Windward Side of Sweptback Injectors at Angle of Attack," *Journal of Spacecraft and Rockets,* Vol. 8, No. 10, 1971, pp. 1101-1103.

[6]Rogers, R. C., "Mixing of Hydrogen Injected From Multiple Injectors Normal to a Supersonic Airstream," NASA TND-6476, Sept. 1971.

[7]Schetz, J. A., and Billig, F. S., "Penetration of Gaseous Jets Injected into a Supersonic Stream," *Journal of Spacecraft and Rockets,* Vol. 3, No. 11, Nov. 1966, pp. 1658-1665.

[8]Kenworthy, M., and Schetz, J. A., "An Experimental Study of Slot Injection into a Supersonic Stream," *AIAA Journal,* Vol. 11, No. 5, 1973, pp 585-586.

[9]Schetz, J. A., and Gilreath, H. E., "Tangential Slot Injection in

Supersonic Flow," *AIAA Journal,* Vol. 5, No. 12, 1967, pp. 2149–2154.

[10]Walker, D. A., Campbell, R. L., and Schetz, J. A., "Turbulence Measurements for Slot Injection in Supersonic Flow," AIAA Paper 88-0123, 1988.

[11]Mays, R. B., Thomas, R. H., and Schetz, J. A., "Low Angle Injection into a Supersonic Flow," AIAA Paper 89-2461, July 1989.

[12]Smith, B. R., "Mean Flow Measurements of Heated Supersonic Slot Injection into a High Reynolds Number Supersonic Flow," M.S. Thesis, Virginia Polytechnic Institute and State Univ., Blacksburg, VA, 1989.

[13]King, P. S., "Combined Tangential-Normal Injection into a Supersonic Flow," M.S. Thesis, Virginia Polytechnic Institute and State Univ., Blacksburg, VA, 1989.

[14]Hoerner, S. F., *Fluid Dynamic Drag,* published by the author, 1965.

[15]Crocco, L., and Lees, L., "A Mixing Theory for the Interaction between Dissipative Flows and Nearly Isentropic Steams," *Journal of the Aeronautical Sciences,* Vol. 19, Oct. 1952, pp. 649–676.

[16]Jet Penetration Analysis computer program, Johns Hopkins University Applied Physics Laboratory, 1987, based on Billig, F. S., Orth, R. C., and Lasley, M., "A Unified Analysis of Gaseous Jet Penetration," *AIAA Journal,* Vol. 9, No. 6, 1971.

[17]Schetz, J. A., Hawkins, P. F., and Lehman, H., "Structure of Highly Underexpanded Jets in a Supersonic Stream," *AIAA Journal,* Vol. 5, No. 5, 1966, pp. 882–884.